Research Article Vol. 2, No. 12 / 15 December 2019 / OSA Continuum 3514

OSA CONTINUUM

Orthographic imaging of free-flowing aerosol particles

Jesse C. Laning and Matthew J. Berg*

Department of Physics, Kansas State University, 1228 N. 17th St., Manhattan, KS 66506-2601, USA
**matt.berg@phys.ksu.edu*

Abstract: A method to obtain contact-free images of aerosol particles with digital holography from three orthogonal directions is described and demonstrated. Diode lasers of different wavelengths simultaneously illuminate free flowing particles to form holograms on three sensors. Images of the particles are reconstructed from the holograms and used to infer the three-dimensional structure of single spherical particles or clusters of sphere-like particles. The apparatus employs inexpensive components and requires no lenses to achieve the imaging, which gives it a large sensing volume and simple design.

© 2019 Optical Society of America under the terms of the OSA Open Access Publishing Agreement

1. Introduction

The ability to image particles micrometers in size in a three-dimensional (3D) manner is useful for many applications in medicine, science, and industry [1]. For example, particle-type differentiation, and even identification in some cases, can be aided by the knowledge of a particle's 3D form. Such information is also useful to estimate particle volume. Methods are available to resolve or reconstruct the 3D form of particles of this size, such as confocal microscopy and X-ray, electron, or optical tomographic microscopy [2–7]. In all cases (except [7], which is not optical), these methods require fixing particles to a transparent stage, trapping them optically, or confining them in a liquid. As such, they are not useful in cases where particles must be observed in free space without contact or confinement. Aerosols are one example where contact-free imaging is preferred to avoid shape-related particle collection artifacts, or is required, as is the case for ice or liquid-drop particles.

This article presents an experiment where three two-dimensional (2D) images of several types of free-flowing aerosol particles are obtained using in-line digital holography (DH) without the need to collect, confine, or otherwise trap the particles. Two specific types of particles are considered: Individual spherical glass particles and aggregates of optically opaque sphere-like pollen grains in a non-spherical arrangement. The multiple 2D images are generated by a focusing procedure and are then back-projected into the sensing volume (discussed below) to infer the 3D shape of the particle or cluster. The geometry of a sphere is used as a "base element," or geometric primitive, to express the 3D form because the particles are either spheres or clusters thereof.

In our previous work with DH, a particle or a collection of particles is illuminated by a laser beam and the interference pattern, i.e., hologram, produced by the particle's forward scattered light and the beam is recorded by a CCD sensor [8,9]. Applying Fresnel-Kirchhoff scalar diffraction theory to the hologram then yields a silhouette-like 2D image of the particle from the perspective of the beam direction [10]. By pulsing the laser at the ~200 ns time scale, free-flowing particles can be imaged, and a number of additional useful quantiles can be derived such as the particle's scattering pattern and extinction cross section [11,12].

Other examples of 2D imaging include [13] where laboratory generated aerosols are investigated, and the HOLODEC instrument in [14] where cloud aerosol particles are observed from aircraft in the field. Work that achieves 3D imaging via DH or related methods is found in [15–18]. However, in all of these latter cases, the particles under study are trapped or confined in some

#375142 https://doi.org/10.1364/OSAC.2.003514
Journal © 2019 Received 12 Aug 2019; accepted 20 Nov 2019; published 12 Dec 2019

Research Article Vol. 2, No. 12 / 15 December 2019 / OSA Continuum 3515
OSA CONTINUUM

way such that they reside within the depth of focus of a microscope objective. This restricts the sensing volume to micrometers, or millimeters at most, in the axial direction. The goal here is to establish if DH can provide an approximate realization of the 3D form of a free-flowing *aerosol* particle or cluster of aerosol particles without trapping (or suspension in a liquid) and without lenses such that a large sensing volume is achieved.

2. Experiment

The apparatus shown in Fig. 1 achieves this goal. A hollow mounting cube with 25.4 mm diameter threaded holes through each face is shown in Fig. 1(a). In three of the holes that share a common cube-corner are 25.4 mm diameter lens tubes (although no lenses are used). Mounted to the ends of each tube is a diode laser (DL), each emitting at a different wavelength: $\lambda_r = 660$ nm or "red" for short, $\lambda_g = 520$ nm, or "green," and $\lambda_b = 450$ nm, "blue." The beam path for the blue and green DLs can be seen in the side view in Fig. 1(b). Opposite each DL at the far cube-face is a bandpass filter, corresponding to the DL's wavelength, followed by a board-level monochrome CMOS sensor. A hole ~1 mm in diameter is drilled through the cube along its main diagonal from one apex to another as shown in Fig. 1(a) and 1(b). The hole allows an aerosol stream to be passed from top to bottom through the central region of the cube where the particles are simultaneously illuminated by the three orthogonal DLs and the resulting holograms are recorded.

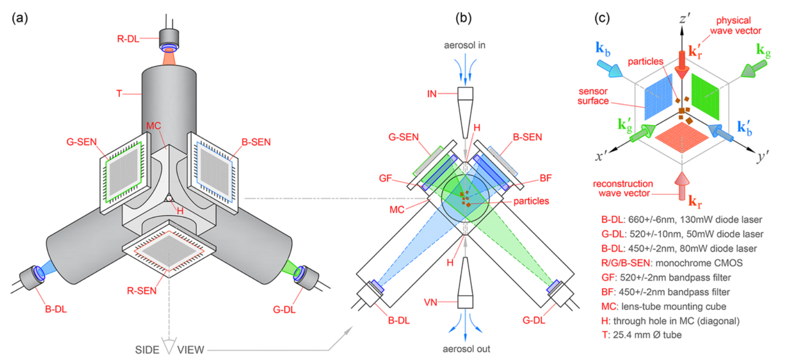

Fig. 1. Sketch of the orthographic imaging apparatus and coordinate systems. In (a), is a top view showing the major components. An aerosol stream is delivered to the sensing volume via a nozzle [shown in (b) as (IN)] through a hole (H) at the top apex of a hollow aluminum "mounting" cube (MC). The particles are removed under negative pressure applied to a corresponding hole and nozzle (VN) at the bottom apex. Lens tubes (T) are connected to each face of the cube as shown. A red, green, or blue diode laser (DL) is mounted at the ends of the three long tubes to illuminate the aerosol flow and three CMOS sensors (SEN) at the opposite cube faces. Guarding each sensor is a bandpass filter matched to the DL opposite the sensor. Two of these filters (GF) and (BF) are visible in (b) where a side view of the apparatus is shown from the perspective indicated in (a). Sketch (b) also shows the unscattered and scattered light from the particles that forms the holograms. Finally, (c) shows the three sensor surfaces defining the SCS, the particles, and the physical and reconstruction wave vectors, $\mathbf{k}'_n$ and $\mathbf{k}_n$.

Board-level sensors are used to allow the hologram recording to be as close to the aerosol stream as practical, which improves the eventual image resolution and gives the apparatus a small form-factor of approximately 10×10×10 cm. These sensors (FLIR, BFS-U3-50S5-BD) have an array size of 2448×2048 pixels, with a pixel size of 3.45×3.45 µm, and a global shutter readout. Clear hologram fringes are recorded by pulsing the DLs simultaneously to emit for a 200 ns period after the electronic-shutter activation, having the effect of freezing-out the particle motion.

OSA CONTINUUM

The purpose of the bandpass filters is to ensure that only light from the DL across the cube from a sensor reaches that sensor's surface. In other words, the filters prevent optical "cross talk" between the sensors. This is preferable to pulsing the DLs sequentially because the likelihood that the particles would change orientation between each pulse.

Because each hologram is formed by illuminating the same group of particles from a different orthogonal direction, the 3D form of a given particle can be inferred from the 2D images, or "views," that are reconstructed from each hologram. As will be seen below, this inference is incomplete and only approximate, yet is vastly better than what is typically achieved from a *single* viewing direction in *lensless* DH.

Particle-image reconstruction begins with a background measurement, which is simply an exposure of the sensors to the DL pulses when no particles are present. This background is then subtracted from the same measurement when the particles are present. The result is a contrast hologram I^{con} of which there are three corresponding to the orthogonal views: $I^{\mathrm{con}}_{\mathrm{r}}$, $I^{\mathrm{con}}_{\mathrm{g}}$, and $I^{\mathrm{con}}_{\mathrm{b}}$. Both the particle-free and particle-present exposures are obtained with synchronized DL pulses ∼200 ns in duration. Each contrast hologram is then used in the Fresnel-Kirchhoff integral [10,19],

$$K_n(\eta,\xi) = \gamma_n \iint_S I^{\mathrm{con}}_n(\eta',\xi')g(\eta,\xi,\eta',\xi')d\eta' d\xi', \tag{1}$$

which is simplified here by use of the Fresnel approximation in that

$$g(\eta,\xi,\eta',\xi') = exp\left\{\frac{ik_n}{2d_n}[(\eta-\eta')^2+(\xi-\xi')^2]\right\}. \tag{2}$$

In Eqs. (1)–(2), $n = \{\mathrm{r},\mathrm{g},\mathrm{b}\}$ to denote the three DL wavelengths λ_n, $\gamma_n = id_n/\lambda_n$, $k_n = 2\pi/\lambda_n$, S is the surface of the n^{th} sensor where contrast hologram I^{con}_n is measured, and d_n is the particle-sensor separation, or "focus distance," for the n^{th} view. Evaluating $|K_n|^2$ gives the 2D particle image for n^{th} view by iteratively adjusting the value of d_n until the image develops a clear focus using a simple sharpness metric described in [16,20].

The 2D views must then be assessed in 3D space in a way that best conveys a particle's 3D form. To explain how this is done, refer to Fig. 1(c) where the sensor surfaces are shown in the sensor coordinate system (x',y',z'), abbreviated as SCS, along with the corresponding DL wave vectors, $\mathbf{k}'_n$. Equation (1) is evaluated for each I^{con}_n using auxiliary coordinates (η',ξ') and a reconstruction wave vector $\mathbf{k}_n = -\mathbf{k}'_n$, where the coordinate associated with $\mathbf{k}_n$ is perpendicular to the (η',ξ') plane. The particle images then reside in the particle coordinate system (x,y,z), or PCS. For example, consider the red viewing direction, $n = \mathrm{r}$. Here, the auxiliary coordinates would be $\eta' = x'$ and $\xi' = y'$ because $I^{\mathrm{con}}_{\mathrm{r}}$ resides in the (x',y') plane in the SCS. If the physical wave vector $\mathbf{k}'_{\mathrm{r}} = k_{\mathrm{r}}\hat{z}$ were used to evaluate Eq. (1), the particle image would be generated in the $(\eta = x, \xi = y)$ plane in the PCS at a distance d_{r} along the *negative* z-axis, i.e., one obtains the virtual particle-image. Using the reconstruction wave vector $\mathbf{k}_{\mathrm{r}}$ generates the image along the positive z-axis where the particles actually reside. In other words, the reconstruction uses the backpropagation of the DL light. Alternatively, $\mathbf{k}'_{\mathrm{r}}$ can be used provided $d_{\mathrm{r}} \rightarrow -d_{\mathrm{r}}$, which can be seen to have the same effect from Eq. (2).

3. Results

Once reconstructed, the three 2D images are positioned in the PCS such that each corresponds to the geometric projection of the particles along a given viewing direction. Figure (2) shows an example. Here, the particles are a powder of glass microspheres with mean radii of $R_{\mathrm{s}} = 25$ μm that are aerosolized and passed to the injection nozzle (IN) in Fig. (1). A large number of particles pass through the beams at ∼1 m/s velocity and are removed by another nozzle (VN) by a weak vacuum line. Simultaneously pulsing the DLs results in the contrast holograms shown in Fig. 2(a),

OSA CONTINUUM

which are color-coded to match the DL wavelengths. Each exhibit an intricate fringe pattern with features associated with individual particles. Application of Eq. (1) to these holograms yields the orthographic images shown in Fig. 2(b) in the PCS where the silhouettes are color coded similar to Fig. 2(a). Note that the holograms in Fig. 2(a) are slightly cropped to a square size of 2048×2048 pixels rather than the full-sensor size of 2448×2048 pixels.

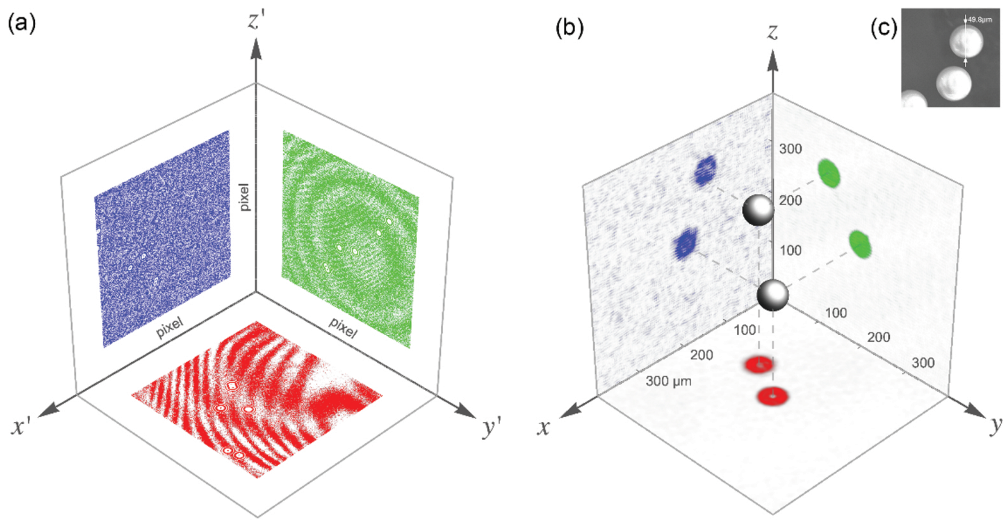

Fig. 2. Orthographic imaging of free-flowing 50 µm diameter spherical aerosol particles. In (a), the contrast holograms I_r^{con}, I_g^{con}, and I_b^{con} are shown color-coded to denote the DL wavelength. Evaluating Eq. (1) as described in the text generates the 2D particle silhouettes for each viewing direction, shown in (b). The holograms and silhouettes are color-coded to match the DL light. The dashed lines show how the center points of the silhouettes are back-projected into 3D space to identify the location of each particle, where a sphere is then drawn. In (c) is an electron micrograph of the glass sphere with ~50 µm diam.

By surveying the relative positions of all silhouettes in the three views in the PCS, it is usually possible to identify a "fiducial" silhouette in each view that corresponds to the same, single particle. A circle is then drawn enclosing this silhouette in each view, defining three radii R_r, R_g, and R_b. From each radius, a scale factor α_n is determined such that the radii equal the *known* particle size, i.e., $\alpha_r R_r = \alpha_g R_g = \alpha_b R_b = R_s$. This procedure addresses the different image-magnification effects due to the different wavelengths and the divergence of the DL beams, which is approximately 10°. The centers of these circles allow the views to be correctly positioned in the PCS by translating each image in its own plane such that back projection of the circles corresponds to the center of a single spherical particle. Figure 2(b) shows dashed lines denoting this back-projection to two spheres from the corresponding view silhouettes. Note that the 3D sphere shapes here are artificially drawn, i.e., they are geometric primitives, while the silhouettes are *real* images that validate the use of these primitives.

Once the scale factors α_n are identified, other particle types can be investigated with the PCS axes now scaled to micrometers. An example is presented in Fig. 3 where a powder of dried, dead ragweed pollen grains is used as the particle source. These are sphere-like particles approximately 20 – 30 μm diameter with an echinate surface that promotes clustering of individual grains. As such, the use of spheres as geometric primitives is again justified. The contrast holograms are presented in Fig. 3(a) and the resulting views are shown in Fig. 3(b). As before, a circle enclosing the silhouette of a single cluster is drawn in each view and the views are then positioned in 3D space via the circles' centers in the PCS. Once positioned, 22 μm diameter spheres are placed in the PCS such that their projections onto the image planes approximately agree with the silhouettes. This sphere size is determined from the blue and green views where outlines of individual grains in most of the cluster can be discerned. Figure 3(b) shows the result of this process where the blue and green-views are included as insets. Close inspection reveals a small degree of misalignment between the spheres and projections, which is more an effect of parallax than misplacement. Small-scale features of the cluster are not captured by this process such as the surface roughness of individual grains and void spaces between grains. This is due to the limited image-resolution of the apparatus, which is estimated as 10 μm from the features that do appear clear in Fig. 3(b). One can also see a lone grain silhouette in the green view in Fig. 3(b) indicated by (*) that is not seen in the other views, and thus, is not represented by a sphere.

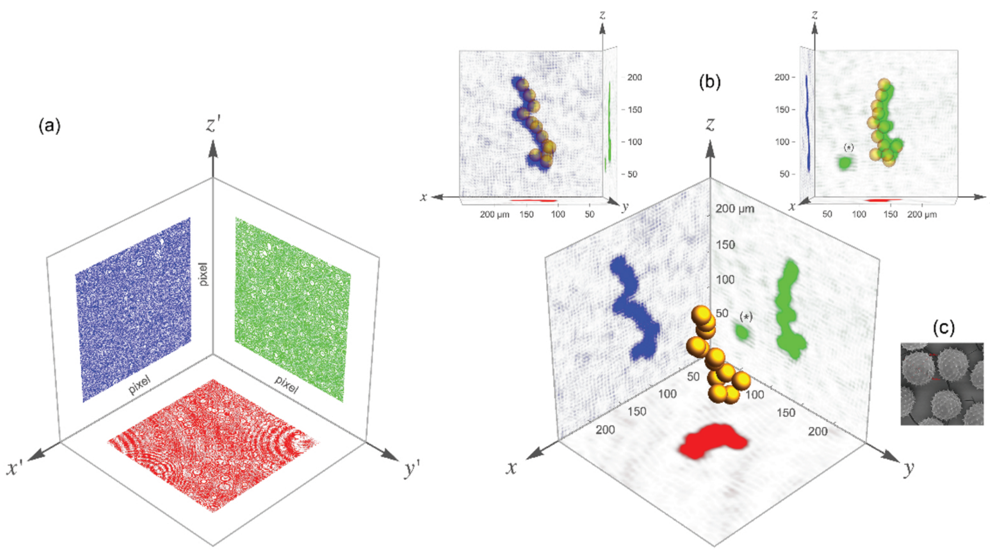

Fig. 3. Orthographic imaging of a ragweed pollen aerosol. In analogy to Fig. 2, (a) shows the contrast holograms and (b) shows the particle silhouettes generated from those holograms for a single particle-cluster. Following alignment of the 2D views via inscribing circles as described in the text, sphere primitives of equal size are placed in 3D space such that their projections onto each of the image planes best agree with the structure seen in each silhouette. To provide more detail, (b) also shows different perspectives of the blue and green views to highlight the correspondence between the silhouettes and the placement of the spheres. The isolated pollen grain labeled (*) is not associated with a sphere because it is visible only in the green view. Image (c) shows an electron micrograph of the pollen grains, which are ~21-22 μm diam.

The utility of this imaging approach can be appreciated from Fig. 3(b) in that if one were provided a single view only, it would be unlikely to generate a reasonable 3D rendering of the full particle-cluster. Consider the red view in Fig. 3(b) as an example. While this view gives an approximate sense for the overall size of the cluster, is does not clearly reveal that the particle is a cluster of spherical grains like the other views do. Indeed, from the red view alone, one may not realize the comparatively long extent of the cluster along the z-axis (axial direction for this view).

The knowledge of the 2D image of the *same* cluster from the different orthogonal directions is the key property that allows this method to work. For example, consider the red viewing direction in Fig. 3(b) again. The individual pollen grains of the cluster have different axial and transverse positions with respect to the z-axis that obscure their 3D location. All that can be determined from the red view is the transverse location of an undetermined number of overlapping sphere primitives; the axial positions are completely obscured and some are not well focused. However,

OSA CONTINUUM

when this same cluster is viewed from the other directions, the transverse locations become known for those views, which identifies the correct axial position for the obscured view. It is then possible to infer the locations of all the spheres. Of course, this approach cannot work if the image resolution prevents a clear silhouette, and it would not be possible to resolve the location of a particle that is obscured by other particles in all three views. The latter case could occur for more compact clusters and aerosol streams involving a large number density of particles.

4. Discussion

A useful aspect of this method is the absence of lenses, which gives it nearly an order of magnitude larger sensing volume than what is typically possible in conventional microscopy. In principle, any particle that occupies the overlap volume of the three DL beams, which is approximately 1 cm^3, will contribute to the holograms and can be imaged in this way.

While the idea to use multiple silhouettes to obtain 3D information of particle form is not new, the application to free-flowing aerosols with all three orthogonal views is. All comparable methods other than [13] (where two views are obtained in a non-holographic way) require either fixing, trapping, or confinement of the particles. In one example, which is partly similar to the approach here, [21] achieves multiple views of sub-millimeter sized objects that are either stationary or slowed in their motion by suspension in a liquid. However, that work employs a clever, yet planar, design that in essence is equivalent to two of the three viewing direction here. Moreover, aerosol particles are not investigated in [21]. Microscope objectives are employed in many designs (although not in [21]) resulting in a much-reduced sensing volume. Applying such methods to free flowing aerosol particles would be difficult because the particle motion even in moderate flow velocities (~1m/s) will washout the hologram interference pattern unless pulsed illumination is used on the 100's of ns time scale. Also, note that the pollen grains in Fig. 3 are opaque, and thus the attractive methods based on transparent phase objects, such as biological cells in water, have not been applied to such aerosol particles as far as we know.

Improvements to this work could include a test of more formal rendering techniques, such as weighted back-projection, to better represent the 3D form of the particles without the use of geometric primitives [3]. The method could also be useful in a practical context. At this time, there are no commercial instruments that determine the shape of freely flowing aerosol particles. Given the design simplicity, small form-factor, and large sensing volume of the apparatus in Fig. 1 we suggest that such instruments could be developed and that significant advancements could be achieved in aerosol science by deploying the instruments on an unmanned aerial vehicles.

Funding

Directorate for Geosciences (1665456); Air Force Office of Scientific Research (FA9550-19-1-0078).

Acknowledgments

The authors are grateful for helpful discussions with Stephen Holler, Sungsoo S. Kim, Gorden Videen, the KSU Electronics Design Laboratory, and Andrew Thurlow for machining services.

Disclosures

The authors declare that there are no conflicts of interest related to this article.

References

1. P. Kulkarni and K. Willeke (eds.), *Aerosol Measurement: Principles, Techniques, and Applications* (Wiley, New Jersey, 2011), p. 752.

OSA CONTINUUM

2. F. Joachim, (ed.) Electron Tomography: Methods for Three-Dimensional Visualization of Structures in the Cell, 2nd ed., (Springer, New York, 2006).
3. A. J. Koster, U. Ziese, A. J. Verkleij, A. H. Janssen, and K. P. de Jong, "Three-dimensional transmission electron microscopy: A novel imaging and characterization technique with nanometer scale resolution for material science," J. Phys. Chem. B **104**(40), 9368–9370 (2000).
4. D. Jin, R. Zhou, Z. Yaqoob, and P. T. C. So, "Tomographic phase microscopy: Principles and applications in bioimaging [invited]," J. Opt. Soc. Am. B **34**(5), B64–B77 (2017).
5. F. Merola, P. Memmolo, L. Miccio, M. Mugnano, and P. Ferraro, "Phase contrast tomography at lab on chip scale by digital holography," Methods **136**, 108–115 (2018).
6. Y.-L. Pan, C. Wang, S. C. Hill, M. Coleman, L. A. Beresnev, and J. L. Santarpia, "Trapping of individual airborne absorbing particles using a counterflow nozzle and photophoretic trap for continuous sampling and analysis," Appl. Phys. Lett. **104**(11), 113507 (2014).
7. N. D. Loh, C. Y. Hampton, A. V. Martin, D. Starodub, R. G. Sierra, A. Barty, A. Aquila, J. Schulz, L. Lomb, J. Steinbrener, S. Shoeman, R. L. Kassemeyer, C. Bostedt, J. Bozek, S. W. Epp, B. Erk, R. Hartmann, D. Rolles, A. Rudenko, B. Rudek, L. Foucar, N. Kimmel, G. Weidenspointner, G. Hauser, P. Holl, E. Pedersoli, M. Liang, M. Hunter, L. Gumprecht, N. Coppola, C. Wunderer, H. Graafsma, F. R. N. C. Maia, T. Ekeberg, M. Hantke, H. Fleckenstein, H. Hirsemann, K. Nass, T. A. White, H. J. Tobias, G. R. Farquar, W. H. Benner, S. Hau-Riege, C. Reich, A. Hartmann, H. Soltau, S. Marchesini, S. Bajt, M. Barthelmess, P. Bucksbaum, K. O. Hodgson, L. Strüder, J. Ullrich, M. Frank, I. Schlichting, H. N. Chapman, and M. J. Bogan, "Fractal morphology, imaging and mass spectrometry of single aerosol particles in flight," Nature **486**(7404), 513–517 (2012).
8. M. J. Berg and G. Videen, "Digital holographic imaging of aerosol particles in flight," J. Quant. Spectrosc. Radiat. Transfer **112**(11), 1776–1783 (2011).
9. M. J. Berg, Y. W. Heinson, O. Kemppinen, and S. Holler, "Solving the inverse problem for coarse-mode aerosol particle morphology with digital holography," Sci. Rep. **7**(1), 9400 (2017).
10. T. Kreis, Handbook of Holographic Interferometry: Optical and Digital Methods (Wiley, 2005), p.96.
11. M. J. Berg, N. R. Subedi, and P. A. Anderson, "Measuring extinction with digital holography: Nonspherical particles and experimental validation," Opt. Lett. **42**(5), 1011–1014 (2017).
12. R. Giri, C. Morello, Y. W. Heinson, O. Kemppinen, G. Videen, and M. J. Berg, "Generation of aerosol-particle light-scattering patterns from digital holograms," Opt. Lett. **44**(4), 819–822 (2019).
13. M. Brunel, B. Delestre, and M. Talbi, "3D-reconstructions for the estimation of ice particle's volume using a two-views interferometric out-of-focus imaging set-up," Rev. Sci. Instrum. **90**(5), 053109 (2019).
14. J. P. Fugal, R. A. Shaw, E. W. Saw, and A. V. Sergeyev, "Airborne digital holographic system for cloud particle measurements," Appl. Opt. **43**(32), 5987–5995 (2004).
15. A. Brodoline, N. Rawat, D. Alexandre, N. Cubedo, and M. Gross, "4D compressive sensing holographic imaging of small moving objects," Opt. Lett. **44**(11), 2827–2830 (2019).
16. O. Kemppinen, Y. Heinson, and M. J. Berg, "Quasi three-dimensional particle imaging with digital holography," Appl. Opt. **56**(13), F53–F60 (2017).
17. S. Kara-Mohammed, L. Bouamama, and P. Picart, "Imaging of particles with 3D full parallax mode with two-color digital off-axis holography," Opt. Laser Eng. **104**, 53–61 (2018).
18. F. Merola, L. Miccio, P. Memmolo, G. Di Caprio, A. Galli, R. Puglisi, D. Balduzzi, G. Coppola, P. Netti, and P. Ferraro, "Digital holography as a method for 3D imaging and estimating the biovolume of motile cells," Lab Chip **13**(23), 4512–4516 (2013).
19. S. Holler, M. J. Berg, O. Kemppinen, and Y. W. Heinson, "Two-dimensional scattering and digital holography from isolated aerosol particles," *Proc. SPIE 10669, Computational Imaging III*, 106690B (2018).
20. F. Dubois, C. Schockaert, N. Callens, and C. Yourassowsky, "Focus plane detection criteria in digital holography microscopy by amplitude analysis," Opt. Express **14**(13), 5895–5908 (2006).
21. L. Williams, G. Nehmetallah, and P. P. Banerjee, "Digital tomographic compressive holographic reconstruction of three-dimensional objects in transmissive and reflective geometries," Appl. Opt. **52**(8), 1702–1710 (2013).

24.255.140.223 {ts '2019-12-13 00:23:27'}